Title: Translation of monosynaptic circuits underlying amygdala fMRI neurofeedback training

Running Title: Monosynaptic circuits underlying amygdala neurofeedback

Authors: Lucas Trambaiolli[1,2], Chiara Maffei[3,4], Evan Dann[3], Claudinei Biazoli Jr[5,6], Gleb Bezgin[7], Anastasia Yendiki[3], Suzanne Haber[1,2]

Affiliations:
1 - McLean Hospital, Harvard Medical School, U.S.A.
2 - Department of Pharmacology and Physiology, University of Rochester, U.S.A.
3 - Athinoula A. Martinos Center for Biomedical Imaging, Massachusetts General Hospital and Harvard Medical School, U.S.A.
4 - Center for Neurotechnology and Neurorecovery, Department of Neurology, Massachusetts General Hospital, USA.
5 - Center for Mathematics Computation and Cognition, Federal University of ABC, Brazil.
6 - School of Biological and Behavioural Sciences, Queen Mary University of London, U.K.
7 - Neuroinformatics for Personalized Medicine lab, Montreal Neurological Institute, McGill University, Montréal, QC, Canada.

Corresponding authors:
Lucas Trambaiolli, ltrambaiolli@mclean.harvard.edu
Suzanne Haber, suzanne_haber@urmc.rochester.edu

***Abstract*:**
Background. fMRI neurofeedback targeting the amygdala is a promising therapeutical tool in psychiatry. It induces resting-state functional connectivity (rsFC) changes between the amygdala and regions of the salience and default mode networks (SN and DMN, respectively). We hypothesize these rsFC changes happen on the amygdala's underlying anatomical circuits.
Methods. We used the coordinates from regions of interest (ROIs) from studies showing pre-to-post-neurofeedback changes in rsFC with the left amygdala. Using a cross-species brain parcellation, we identified the homologous locations in non-human primates. We injected bidirectional tracers in the amygdala of adult macaques and used bright- and dark-field microscopy to identify cells and axon terminals in each ROI. We also performed additional injections in specific ROIs to validate the results following amygdala injections and delineate potential disynaptic pathways. Finally, we used high-resolution diffusion MRI data from four *post-mortem* macaque brains and one *in vivo* human brain to translate our findings to the neuroimaging domain.
Results. The amygdala had significant monosynaptic connections with all the SN and DMN ipsilateral ROIs. Amygdala connections with the DMN contralateral ROIs are disynaptic through the hippocampus and parahippocampal gyrus. Diffusion MRI in both species benefitted from using the ground-truth tracer data to validate its findings, as we identified false-negative ipsilateral and false-positive contralateral connectivity results.
Conclusions. Amygdala neurofeedback modulates the SN and DMN through monosynaptic connections and disynaptic pathways - including hippocampal structures involved in the neurofeedback task. Neurofeedback may be a tool for rapid modulation and reinforcement of these anatomical connections, leading to clinical improvement.

***Keywords*:** Neurofeedback, functional connectivity, resting-state, non-human primates, tract-tracing, tractography, neuroanatomy.

Introduction

Functional Magnetic Resonance Imaging (fMRI) neurofeedback modulates specific brain regions in real time through self-elicited mental strategies [1]. It is considered a potential therapeutic approach in psychiatry for several disorders, including depression, anxiety, and substance abuse [2-4]. Comparing resting-state functional connectivity (rsFC) before and after neurofeedback provides insights into which brain networks support the long-lasting effects of neuromodulation [5, 6]. However, fMRI is an indirect method for connectivity analysis. Delineating the hard-wired, monosynaptic connections that underlie these rsFC results will lead to: (i) identifying the circuitries underlying neurofeedback mechanisms; (ii) probing those circuits with animal models; (iii) developing potential biomarkers; (iv) guiding personalized neurofeedback protocols. This study aims to determine the extent to which rsFC changes elicited by neurofeedback modulation represent changes in anatomic, monosynaptic connections. We use NHP anatomic tracing experiments and high-resolution diffusion MRI (dMRI) data in macaques and humans to determine the most likely monosynaptic connectivity changes following neurofeedback intervention.

We focused on connectivity changes following fMRI neurofeedback of the amygdala, a successful neurofeedback target [7, 8]. The current hypothesis is that clinical improvement following amygdala neurofeedback results from its modulation of two large-scale networks: the salience and the default mode networks (SN and DMN, respectively) [8-12]. Although connections between the amygdala and SN and DMN nodes have been described [13-34], these are large regions with several subdivisions, each with different connectivity patterns [15, 23, 24, 27, 29, 30]. Here, we combined multi-modal multi-species data to delineate the anatomical circuits connecting the amygdala and the specific DMN and SN sublocations (or regions-of-interest - ROIs) modulated by amygdala neurofeedback [5, 12, 35]. Specifically, we: *1.* Identified the equivalent ROIs in the non-human primate (NHP) brain. *2.* Analyzed the anatomical connections between each sublocation and the amygdala. *3.* Tested whether the same connections could be identified using submillimeter *ex vivo* dMRI tractography data in NHP. *4.* Tested whether these connections could also be identified in human submillimeter *in vivo* dMRI.

Our results show that the main rsFC changes following neurofeedback are likely sustained by monosynaptic connections between the amygdala and ipsilateral ROI sublocations of the SN and DMN nodes. Amygdala connections with contralateral ROIs are disynaptic, likely through hippocampal and parahippocampal gyrus (PHG) regions involved in neurofeedback tasks [11, 36, 37]. This anatomical delineation allows for future neurofeedback studies probing those circuits and related mechanisms in human and animal models and using neurofeedback to identify biomarkers or personalized targets in clinical samples.

Methods

Step 1: Translating rsFC ROIs from human to the NHP brain

We extracted the rsFC ROIs from all three studies [5, 12, 35] that used seed-based connectivity analysis to evaluate an fMRI neurofeedback protocol based on positive autobiographical memory recall to up-regulate the BOLD signal of the left amygdala. There were 16 ROIs (Table 1) in which rsFC with the left amygdala changed after neurofeedback, including some, but not all, ROIs of the SN (dorsal anterior cingulate cortex - dACC, anterior insula – AI, and lateral prefrontal cortex - LPFC) and DMN (middle frontal gyrus - MFG, temporal pole - TP, hippocampus, parahippocampal gyrus – PHG, precuneus, posterior cingulate cortex – PCC and thalamus). The coordinates of these ROIs were transformed to the MNI space based on Lancaster, et al. [38].

Original ROI label	**Human coordinates (MNI space)**			**NHP coordinates (F99 space)**		
	x	y	z	x	y	z
Ipsilateral (Left Hemisphere) Salience Network nodes						
Dorsal anterior cingulate cortex (dACC)	-2	25	30	-2	10	15
Lateral prefrontal cortex (LPFC)	-50	14	0	-24	7	0
Anterior Insula (AI)	-37	21	5	-21	3	1
Ipsilateral (Left Hemisphere) Default Mode Network nodes						
Middle frontal gyrus	-30	15	44	-13	11	17
Temporal pole	-43	3	-24	-18	3	-6
Parahippocampal gyrus (PHG)	-26	-4	-19	-8	-3	-14
Angular gyrus*	-44	-53	28	-21	-23	15
Medial precuneus*	-7	-59	40	-1	-24	20
Lateral precuneus	-27	-54	46	-14	-23	19
Contralateral (Right Hemisphere) Default Mode Network nodes						
Middle frontal gyrus	28	45	33	17	14	14
Temporal pole	45	18	-29	22	6	-9
Parahippocampal gyrus (PHG)	30	-27	-23	17	-5	-18
Hippocampus	30	-26	-2	15	-12	-8
Posterior cingulate cortex	3	-47	31	2	-23	11
Medial precuneus	13	-31	50	6	-12	17
Thalamus	17	-24	-2	9	-14	-1

Table 1 – List of center or peak coordinates of nodes showing amygdala-rsFC changes when comparing pre- and post-amygdala neurofeedback training in human subjects and the

equivalent coordinates in the homologous structures of the macaque brain. Nodes are grouped as part of the human Salience or Default Mode Networks. Coordinates in the human brain are reported in the MNI brain template (center), and coordinates in the macaque brain in the F99 brain template. * = coordinates estimated based on figures.

We used the "Regional Map" parcellation, a standard for cross-species comparisons [39], to identify equivalent ROIs across NHPs and humans. Details about this parcellation are included in the *Supplementary Information*. The equivalent ROIs in the macaque brain were manually placed according to homologous parcels and anatomical landmarks. Importantly, in this study, we used human terminology when referring to the NHP ROIs (e.g., although we list ROIs in the "angular gyrus" and "middle frontal gyrus" macaques don't have these gyri in the strict sense).

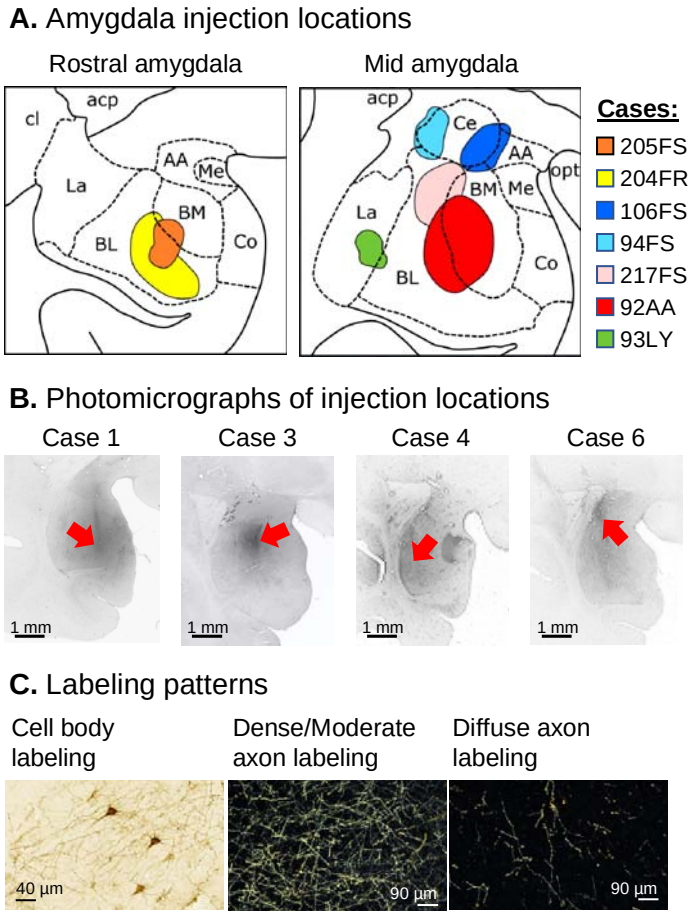

Figure 1 – Amygdala Injection sites and labeling patterns. A. Schematic of injection sites at approximately the same rostro-caudal level in the macaque amygdala. Dotted lines = nuclei borders. Colored areas = individual cases. **B.** Coronal sections of the macaque amygdala showing different injection locations. Scale bar, 1 mm. **C.** Examples of dense/moderate and diffuse terminal fields. *Abbreviations*: AA = Anterior area; acp = anterior commissure - posterior

limb; BL = Basolateral nucleus; BM = Basomedial nucleus; Ce = Central nucleus; cl = claustrum; Co = Cortical nucleus; La = Lateral nucleus; Me = Medial nucleus; opt = optic tract.

Step 2: Identification of anatomical connections using NHP tract-tracer data

Our laboratory has an extensive collection of bidirectional tracer injections placed throughout cortical and subcortical areas of adult male macaque monkeys. From this database, we selected 12 injection sites (four placed in *Macaca mulatta*, four in *Macaca fascicularis*, and four in *Macaca nemestrina*). For the seven injections in the amygdala (Figure 1A), we evaluated connections with each SN and DMN ROIs from Table 1. We used the additional five injections in specific ROIs (anterior insula, lateral precuneus, hippocampus, posterior cingulate cortex, and thalamus) to validate the connectivity patterns with the amygdala. The surgical and histological procedures are detailed in the *Supplementary Information*.

Using StereoInvestigator software (MicroBrightField Bioscience, U.S.A), we charted the retrogradely labeled cells in the ROIs under light-field microscopy at 20 x (Figure 1B, left) [40-42]. We used dark-field microscopy under 1.6 x, 4 x, and 10 x objectives with Neurolucida software (MicroBrightField) to outline dense or light axon terminal projections in the ROIs. We labeled condensed groups of fibers visible at 1.6 x with discernible boundaries as ‘dense projections’ (Figure 1B, center), and groups of fibers where individual terminals could be discerned as ‘light projections’ (Figure 1B, right) [40, 42].

Step 3: Identification of anatomical connections using NHP tractography data

The NHP postmortem submillimeter dMRI data was collected from four adult animals, with a total scan time of 47 hours per brain (MRI acquisition details can be found in the *Supplementary Information*). The dMRI data underwent a preprocessing pipeline that included denoising [43] and correction for Gibbs ringing [44], signal drift [45], eddy-currents [46], and bias fields [47]. We fit fiber orientation distribution functions (fODF) to the pre-processed data using multi-shell multi-tissue constrained spherical deconvolution (MSMT-CSD [48]) in MRtrix3 [47]. The D99 macaque atlas [49] was transformed to each individual brain after registering the D99 magnetization transfer ratio (MTR) template volume to the individual b=0 volume using the robust affine registration in FreeSurfer (mri_robust_register [50]). The left amygdala was extracted from the D99 atlas, binarized, and dilated by 2 voxels in MRtrix3 to include the surrounding white matter. We performed probabilistic tractography in MRItrix3 seeding in every voxel within this mask (350 seeds per voxel). The following tractography parameters were used: step-size = 0.25 mm, maximum angle threshold = 30˚, fODF peak threshold = 0.06, and maximum length = 150 mm.

The location of each rsFC ROI was identified as a single point on the D99 macaque brain based on anatomical landmarks. These point coordinates were mapped

to each individual brain using the transforms from the registration described above. For each point, we found its nearest point along the white-gray matter boundary. Spherical ROIs were defined with a 1.5 mm radius around these points. Streamlines connecting the left amygdala and each of the ROIs included in this analysis were manually dissected using Trackvis (v.0.6.1; http://www.trackvis.org). Streamlines connecting the left amygdala with each ROI were filtered to only include those streamlines ending or originating inside the amygdala mask.

Step 4: Human tractography analysis

We used submillimeter-resolution dMRI data from a publicly available and pre-processed dataset [51] (see details in the *Supplementary Information*). Processing followed similar steps to those previously described for the NHP data. We fit fODFs to the preprocessed dMRI data using multi-shell multi-tissue constrained spherical deconvolution (MSMT-CSD) in MRtrix3. Cortical parcellations and subcortical segmentations were obtained from the T1 data using FreeSurfer [52-54]. The left amygdala was extracted from the segmentation, binarized, and inflated by 1 voxel. We performed probabilistic tractography in MRtrix3, seeding in every voxel within the amygdala (100 seeds per voxel). The following tractography parameters were used: step-size = 0.38 mm, maximum angle threshold = 45°, maximum length = 150 mm. We mapped the ROI coordinates from the MNI space to the individual space using the registration procedures described in the NHP analysis.

Streamlines connecting the left amygdala and each ROI from Table 1 were manually dissected using Trackvis. For the amygdala, a sphere was created around the center coordinates extracted from seed-based rsFC studies [5, 12] . A 10 mm radius was used to include the surrounding white matter. For all other cortical ROIs, spheres of 7 mm radius with their centers at the border between white and gray matter closest to the ROI coordinates.

Results

Step 1: Cross-species ROIs selected for this study

Based on anatomical landmarks, we identified the equivalent 16 ROIs in the NHP brain, and the resulting center coordinates in the F99 space are listed in Table 1. The SN ROIs in the NHP brain included the ipsilateral (left hemisphere) dACC (at the genu of the corpus callosum including area 24, Figure 2A-left), AI (at the rostral portion of the circular sulcus including area AI, Figure 2B-left), and LPFC (caudal area 47/12 extending to ProM at the dorsal lip of the rostral part of lateral fissure Figure 2C-left).

The ipsilateral ROIs of the DMN included the MFG (at the ventral bank of the superior arcuate sulcus, in the border of areas 8AB, 8B, and 9/46D, Figure 3A-left) in

the frontal cortex. In the temporal cortex, the TP (at the ventral bank of the circular sulcus including areas IPro and TPPro Figure 3B-left) and PHG (dorsal to the rhinal fissure, at the border of areas EI, ELC, and ER, Figure 3C-left). Finally, in the parietal cortex, ROIs included the Lateral Precuneus (at the lip of the ventral bank of the intraparietal sulcus, including areas POaE/LIPE and PG, Figure 3D-left), Medial Precuneus (at the ventral bank of the cingulate sulcus, including areas PGm and 31, Figure 3E-left), and Angular Gyrus (AG, in the lateral fissure, including the border of areas PGOp/ReI, PaAC and Tpt, Figure 3F-left).

The DMN ROIs in the contralateral hemisphere included the MFG (at the lower bank of the principal sulcus, including areas 9/46V and 46V) in the frontal cortex. In the temporal cortex, TP (at the dorsolateral portion of the anterior temporal lobe, at area TPPro extending to ST1 - Fig 6A-center) and PHG (at the lateral bank of the rhinal fissure, including areas TLR/R36 and 35 - Fig 6A-right). In the parietal cortex, PCC (area 23 in the cingulate gyrus – Fig 6B) and Medial Precuneus (dorsal bank of the cingulate sulcus, in area 31 extending to areas 23 and 3). And subcortical ROIs include the dorsal Hippocampus (Fig 6A-left) and Thalamus (at the transition between ventral, centromedial, mediodorsal, and pulvinar nuclei – Fig 6C).

Step 2: Anatomical connections identified using NHP tract-tracer data

Bidirectional tracer injections in the amygdala showed monosynaptic connections with the ipsilateral dACC, AI, and LPFC ROIs within the SN Figure 2). Importantly, the basolateral (BL), lateral (La), and lateral central (Ce, case 6) amygdala nuclei, had bidirectional connections with these three ROIs. An anterograde BL injection (Case 7, not shown) was consistent with the spatial patterns of axon terminals observed in the other BL injections. To validate the existence and specificity of the observed connections, we identified a small bidirectional tracer injection in the AI (Figure 4B) that showed bidirectional connectivity patterns spread along all amygdala nuclei, consistent with the results in Figure 2B.

The amygdala was also anatomically interconnected with the ipsilateral DMN sublocations modulated by neurofeedback (Figure 3). ROIs closer to the amygdala (TP and PHG, Figure 3B-C) were bidirectionally connected with all injection locations. The MFG (Figure 3A), precuneus (Figure 3D-E), and angular gyrus (Figure 3F) showed dense labeling with La and Ce injection sites but scarce labeling with BL injections (Cases 2 and 3). None of these DMN ROIs connected with the injection in BL/BM (Case 1). A validation injection in the lateral precuneus (Figure 4C) showed concentrated labeling in the dorsal bank of the amygdala, including the Basal and Ce nuclei. Although this injection is lateral to the original ROI, these results are partially consistent with those observed in the amygdala injections (Figure 3D), except for the lack of labeling in the La nucleus. Importantly, labeling in parietal structures (precuneus and angular

gyrus) after injections in the amygdala and labeling in the amygdala after injection in the precuneus showed predominantly retrograde labeling.

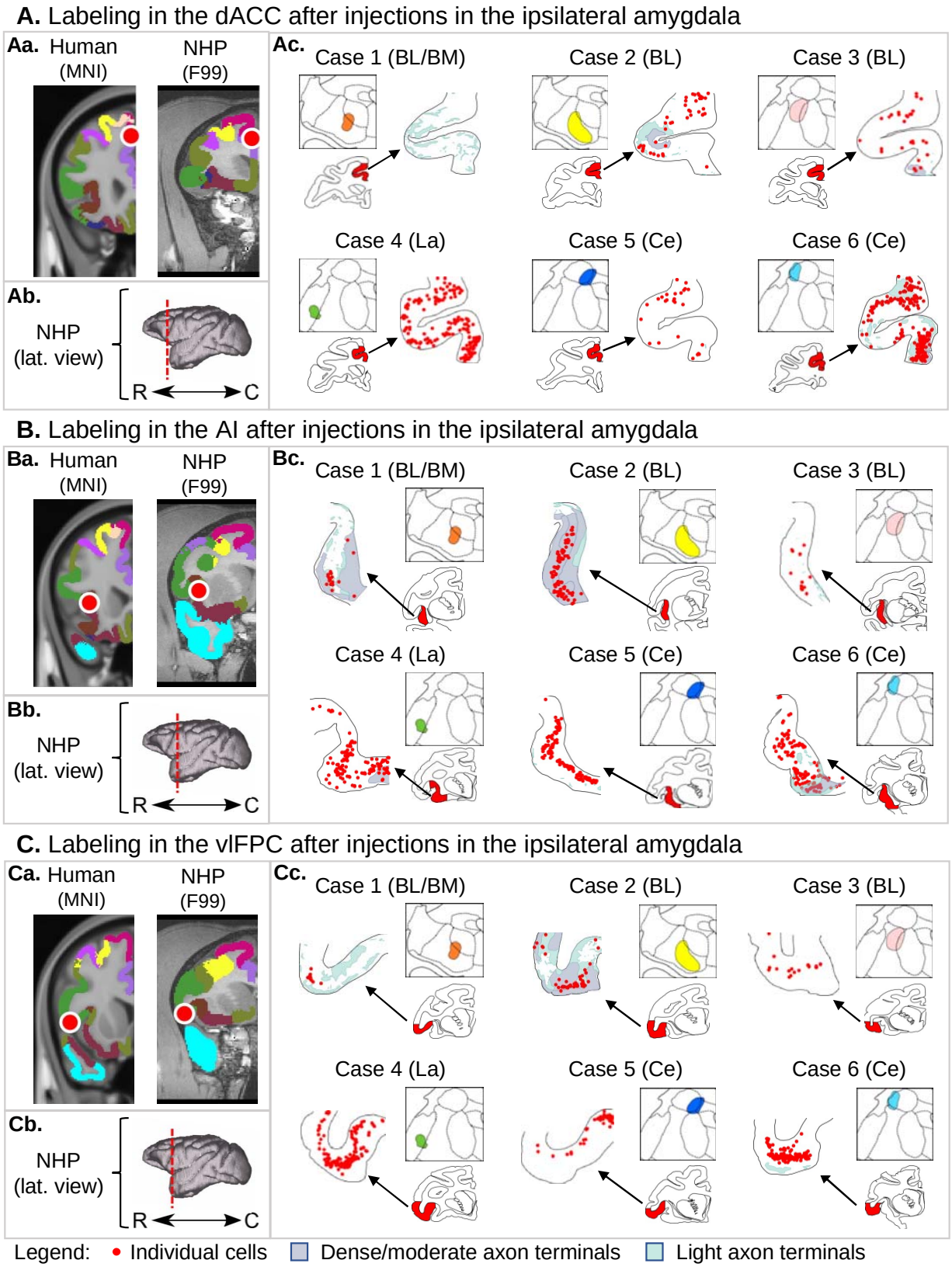

Figure 2 – Amygdala connections with the ipsilateral SN nodes. Aa. Red circles indicate

the peak location of the rsFC changes after amygdala neurofeedback for the dACC in the human MNI template and the homologous location in the macaque F99 template. **Ab.** 3D models represent the rostro-caudal location of coronal slices from each node. **Ac.** For each case, the respective injection is shown in the square box, and the schematic coronal sections highlight in red the location with connectivity chartings. Individual cells are shown as red dots, dense/moderate terminals as light blue shaded areas, and diffuse terminals as light green shaded areas. The same organization is followed for ROIs in the AI (**B**) and vlPFC (**C**). *Abbreviations:* BL = basolateral nucleus, BM = basomedial nucleus, C = caudal, Ce = central nucleus, La = lateral nucleus, R = rostral.

Our tracing data showed sparse monosynaptic connections from the left amygdala to the contralateral hemisphere and no connections with the specific contralateral DMN ROIs. Importantly, amygdala neurofeedback is also associated with changes in the hippocampus and parahippocampal gyrus (PHG) [11, 12, 36, 37, 55], regions also anatomically interconnected with the amygdala [14, 26, 28]. Thus, we evaluated if the amygdala is connected with the contralateral DMN ROIs through the hippocampus and PHG. Supplementary Figure 1B shows anatomical labeling in the left hippocampus and PHG for injections in the left amygdala. Briefly, all cases presented labeling in the amygdalohippocampal area. BL and La injections showed labeling in rostral CA1' and CA3 subfields and dense labeling in the transition between the subiculum and prosubiculum fields, extending to areas 35, 36, and TF in the PHG. A similar but weaker pattern is also observed in Ce (Case 5). A validation injection extending from CA1, ProS, and part of the Subiculum in the hippocampus to areas 35, 36, and TF in the PHG (Supplementary Figure 1C) showed spatial labeling in the amygdala consistent with those observed in Supplementary Figure 1B.

Supplementary Figure 2 illustrates connections between the left hippocampus and PHG and the contralateral DMN ROIs (right hemisphere). Shortly, the injection in the hippocampus and PHG showed anatomical connections with the contralateral hippocampus, PHG, and TP nodes of the DMN (Supplementary Figure 2 A). However, this injection did not include all structures in the hippocampus and PHG. To evaluate if the remaining contralateral DMN nodes listed in Table 1 connected with other hippocampal and PHG subnuclei, we placed two additional injections in two of these nodes: the right PCC (Supplementary Figure 2B) and right thalamus (Supplementary Figure 2C). We observed axon terminal and cell labeling in the left hippocampus and PHG, respectively.

A. Labeling in the MFG after injections in the ipsilateral amygdala

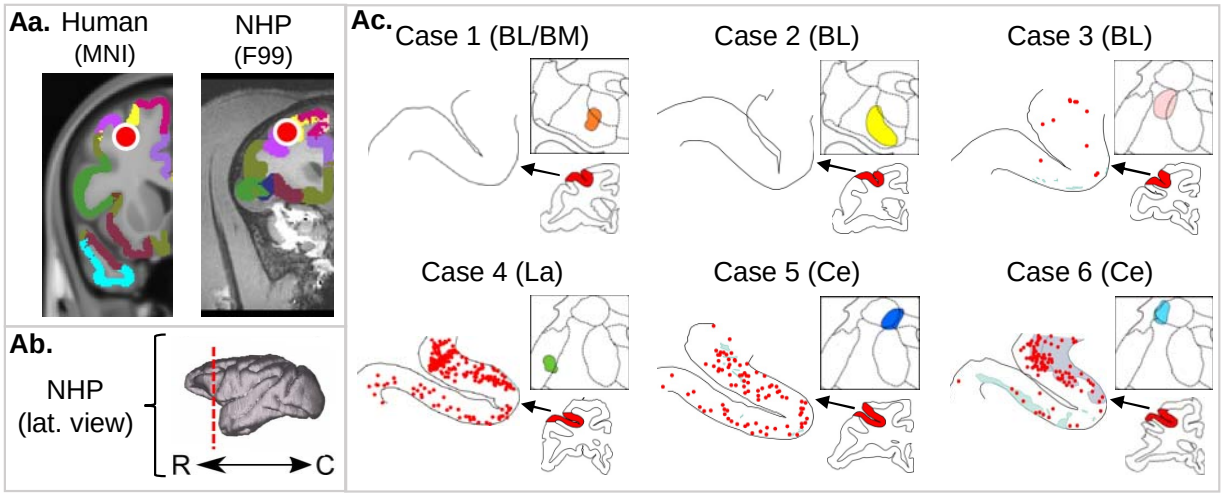

B. Labeling in the TP after injections in the ipsilateral amygdala

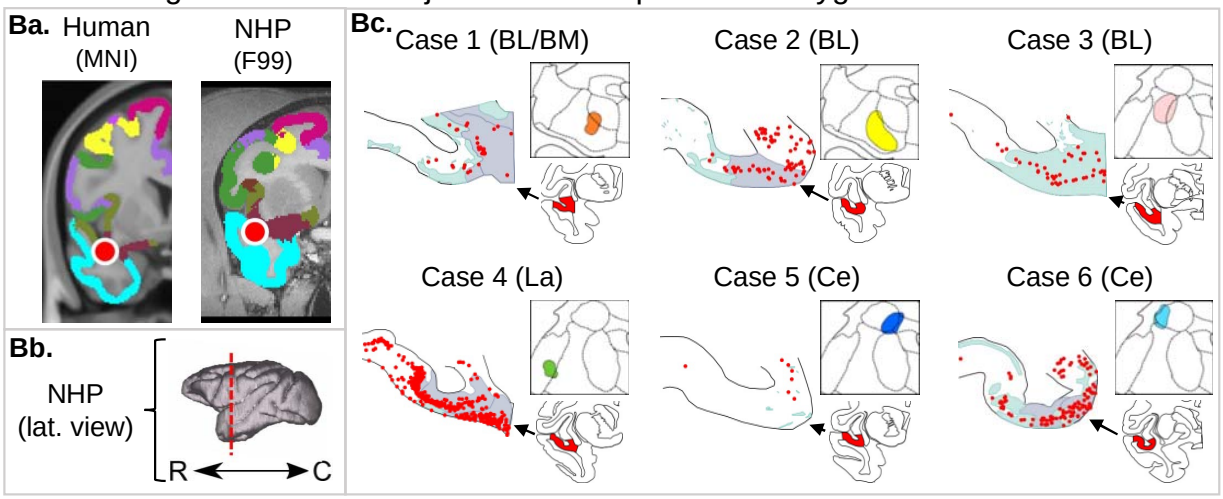

C. Labeling in the PHG after injections in the ipsilateral amygdala

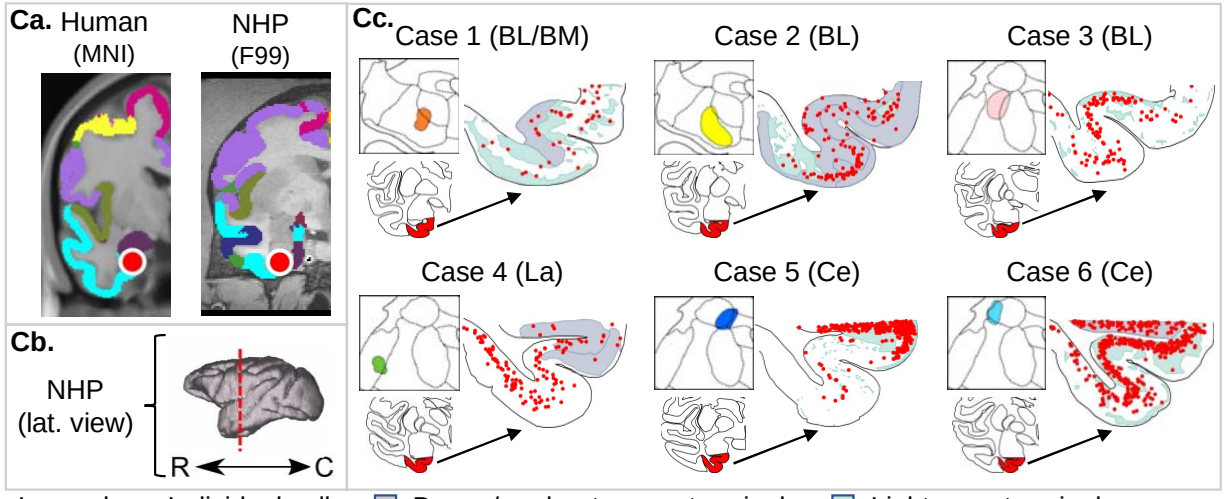

Legend: • Individual cells ▢ Dense/moderate axon terminals ▢ Light axon terminals

D. Labeling in the lateral Precuneus after injections in the ipsilateral amygdala

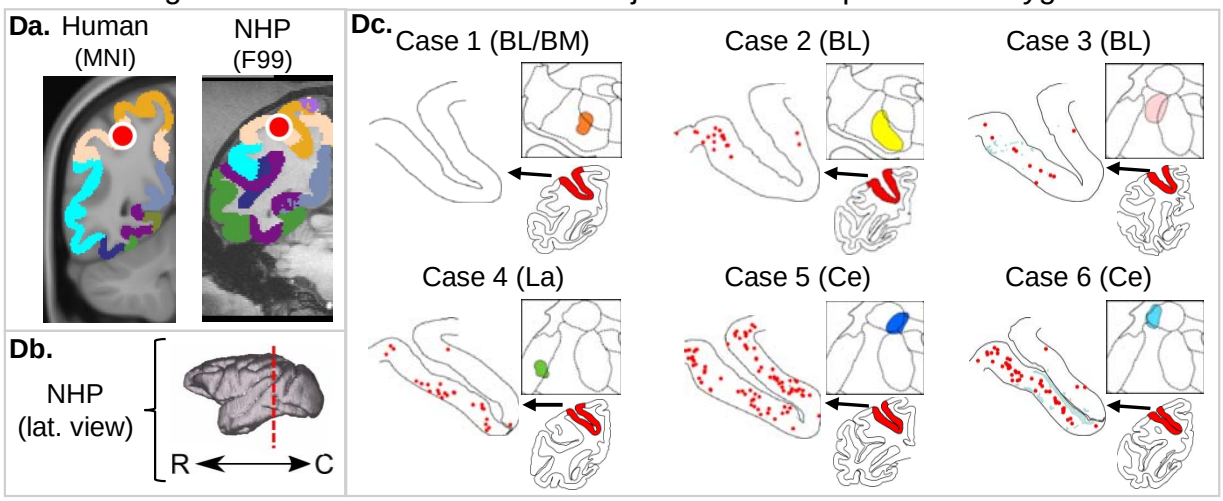

E. Labeling in the medial Precuneus after injections in the ipsilateral amygdala

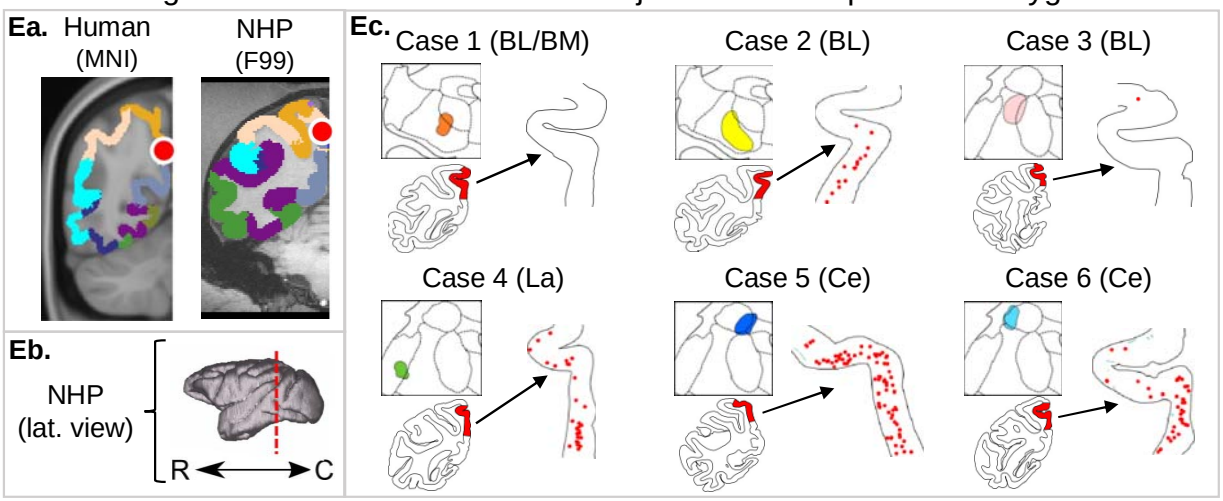

F. Labeling in the Angular Gyrus after injections in the ipsilateral amygdala

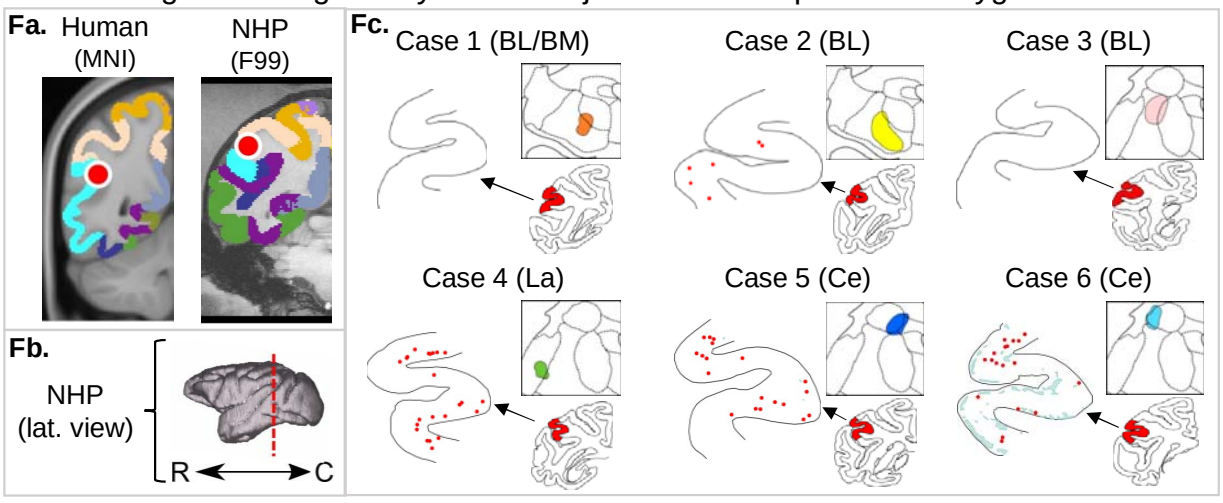

Legend: • Individual cells ▢ Dense/moderate axon terminals ▢ Light axon terminals

Figure 3 – Amygdala connections with the ipsilateral DMN nodes. Aa. Red circles indicate the peak location of the rsFC changes after amygdala neurofeedback for the Middle Frontal Gyrus in the human MNI template and the homologous location in the macaque F99 template. **Ab.** 3D models represent the rostro-caudal location of coronal slices from each node. **Ac.** For each case, the injections in the amygdala are shown in the square box, and the schematic coronal sections highlight the location with connectivity chartings. Individual cells are shown as red dots, dense/moderate terminals as light blue shaded areas, and diffuse terminals as light green shaded areas. The same organization is followed for ROIs in the Temporal Pole (**B**), Parahippocampal Gyrus (**C**), Lateral Precuneus (**D**), Medial Precuneus (**E**), and Angular Gyrus (**F**). *Abbreviations:* BL = basolateral nucleus, BM = basomedial nucleus, C = caudal, Ce = central nucleus, La = lateral nucleus, R = rostral.

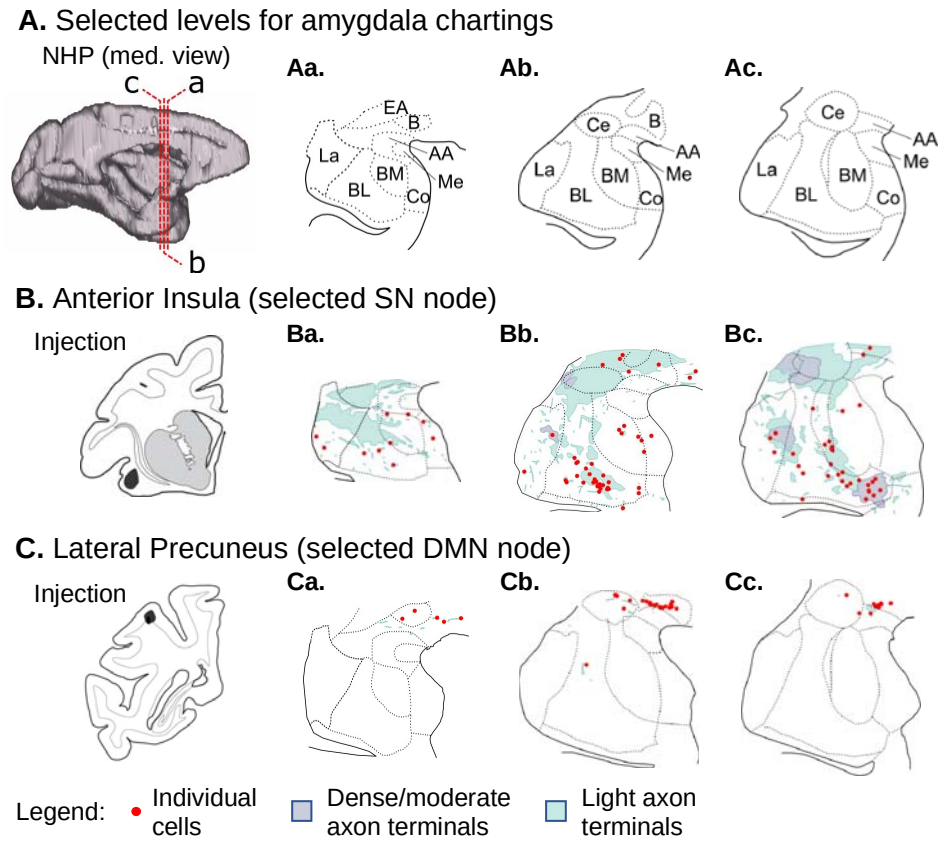

Figure 4 – Validation of amygdala connections after cortical injections. A. 3D representation of the three rostro-caudal levels (a-b) used in the chart cells and terminals in the amygdala, and the respective coronal slices with cytoarchitectonic divisions based on the Paxinos atlas. Labeling of cells (red dots), and dense/moderate (light blue) and diffuse (light green) terminal fields in the amygdala after bidirectional tracer injections in regions homologous to the Anterior Insula (**B**), and Lateral Precuneus (**C**) regions with resting-state functional connectivity changes after amygdala neurofeedback. *Abbreviations:* AA = anterior amygdaloid area. BL = basolateral nucleus, BM = basomedial nucleus, C = caudal, Ce = central nucleus, La = lateral nucleus, R = rostral.

Step 3: Anatomical connections identified with NHP tractography

Using submillimeter dMRI tractography from four animals, we could correctly identify structural connections between the left amygdala and all ipsilateral ROIs. Figure 5 shows examples of well-defined tracts connecting the left amygdala and all ipsilateral ROIs of the SN and DMN in one animal. Additional connections and the results from the other animals are shown in Supplementary Figures 3-5. Importantly, inconsistent with the tracer data, connections between the amygdala and the MFG and LPFC were among those with the fewest streamlines compared to other connections.

Tractography data also showed streamlines connecting the left amygdala with several contralateral ROIs, disagreeing with the tracer data. We compared the tractography and the tracer data at different locations along these tracts to identify where tractography errors occurred. Supplementary Figure 6A shows two sets of streamlines erroneously connecting the left amygdala and the right medial precuneus in one representative case. After leaving the amygdala, the anterior streamlines follow the same direction as the amygdalofugal fibers (Supplementary Figure 6B-C). However, posteriorly, these streamlines enter the fornix (Supplementary Figure 6D), which is inconsistent with the results from the tracer data. The posterior false positive connection follows the same trajectory as the stria terminalis observed in the tracer data (Supplementary Figure 6E-G). However, similar to the anterior false positive, streamlines erroneously follow through the fornix to the contralateral hemisphere.

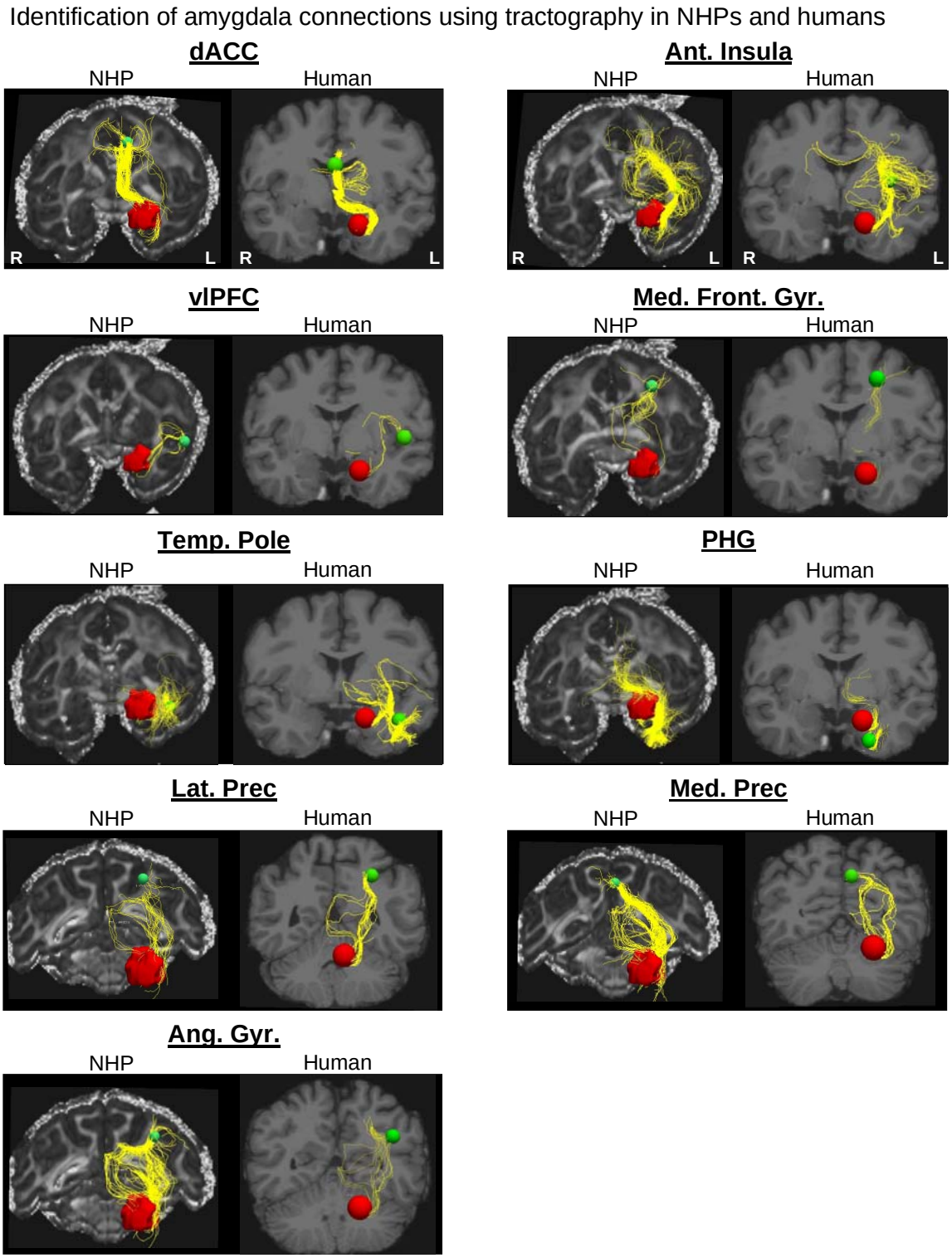

Figure 5 – Identification of amygdala connections using dMRI tractography in NHPs and humans. Reconstruction of streamlines (yellow) connecting the amygdala (red) with all ipsilateral nodes (green) within the SN and DMN. For each node, results from one NHP brain are shown on the left, and results from the human brain on the right.

Step 4: Anatomical connections identified with human tractography

Using submillimeter human dMRI tractography, we successfully identified connections between the left amygdala and all ipsilateral ROIs. Amygdala connections with regions such as the dACC, AI, PHG, TP, and Precuneus showed the same clear tracts with dense concentrations of streamlines (Figure 5) as observed in the NHP dMRI tractography data. Consistent with the NHP dMRI tractography data, amygdala-LPFC, and amygdala-MFG connections presented fewer, sparser streamlines than other connections. Similar to tractography results in NHP, false positive connections were also identified connecting the left amygdala with contralateral ROIs (e.g., streamlines traveling contralaterally through the fornix, Supplementary Figure 6A).

Discussion

Summary

The current mechanistic hypothesis of amygdala neurofeedback is that the amygdala re-directs attention toward salient positive stimuli during self-referential processing, reducing rumination and improving forward-thinking [56, 57]. As observed in task-related and resting-state fMRI, these processes occur via the increased activation and functional connectivity changes in nodes comprising the salience and the default mode networks (SN and DMN, respectively) [9, 11, 36, 57, 58]. Cross-species neuroanatomical homologies [59, 60], including homologous SN [61], and DMN [62, 63] networks in the macaque brain, allow for a deeper delineation of these circuits involved in neurofeedback using NPHs. Previously, the NHP literature showed that the amygdala is anatomically interconnected with the large regions of the SN and DMN nodes [15, 16, 19, 20, 64]. Here, we provide tracer and dMRI evidence that the amygdala has monosynaptic anatomical connections with specific locations within the SN and DMN ipsilateral ROIs modulated by neurofeedback (Figure 6). We also show that amygdala hard-wiring with contralateral DMN ROIs is likely disynaptic through its connections with the adjacent hippocampus and PHG [14, 26, 28], two regions highly active during amygdala neurofeedback training [11, 36, 37]. This circuit delineation allows for new mechanistic descriptions of how the amygdala interactions with the SN and DMN could lead to lasting clinical effects after neurofeedback [8], as discussed below.

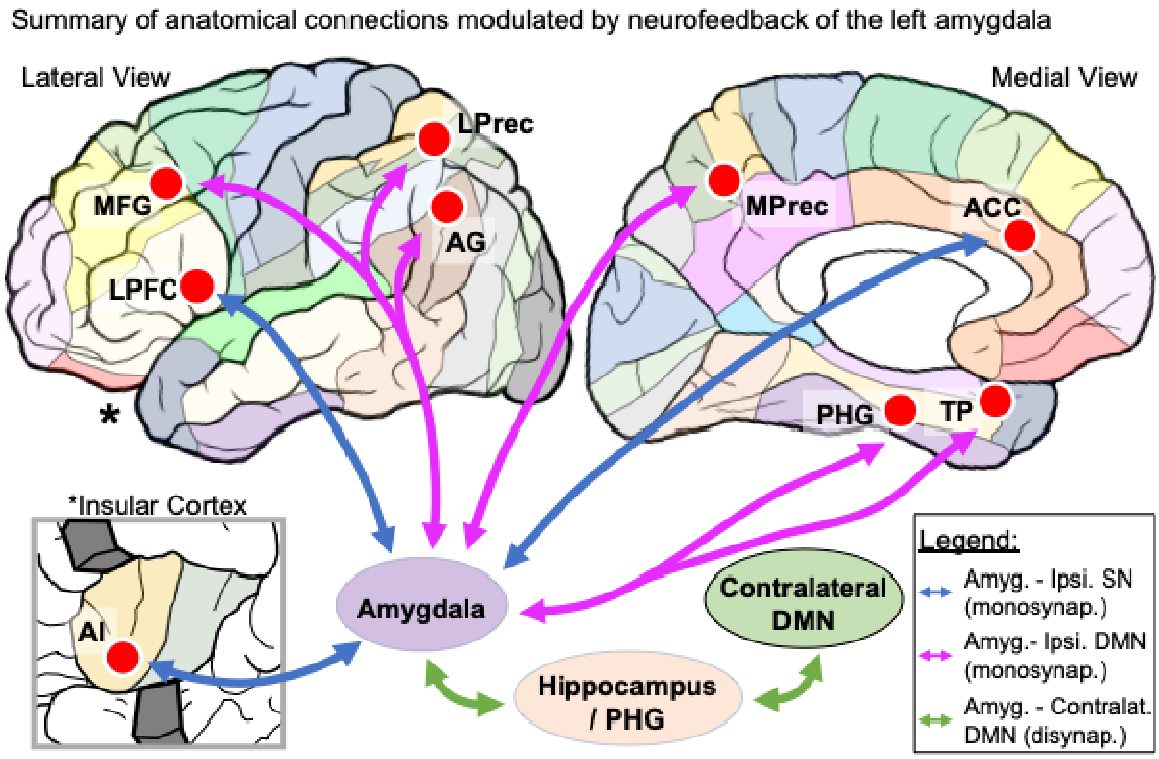

Figure 6 – Summary of anatomical connections modulated by neurofeedback of the left amygdala. Representation of the specificity of ROIs in the left hemisphere (red circles) overlapping major functional regions (colored parcellation). Blue and pink arrows represent monosynaptic connections from the amygdala to the SN and DMN ipsilateral ROIs, respectively. Green arrows show the disynaptic connections with the DMN contralateral ROIs through the hippocampus and PHG.

Amygdaloid connections to the ROIs within the SN and DMN

The amygdala connections to the SN nodes within the frontal and insular cortices are knowingly patchy and terminate in precise areas within each region [15, 19, 20, 22-24, 27, 29, 30]. Our results show that SN ROIs modulated by neurofeedback fall within these patches. These monosynaptic connections support the proposed role of amygdala neurofeedback re-directing attention toward specific salient stimuli [8, 65]. Previous NHP studies support that the amygdala works closely with the SN during salience processing [66-68]. E.g., local stimulation of the amygdala modulates the activity of the ACC and insular ROIs of the SN [69], reinforcing the potential of amygdala modulation of this network through its connections. Brain imaging and lesion studies in humans also highlighted the relevance of the amygdala and its connections in processing emotionally salient stimuli [70-74].

The amygdaloid connections with the DMN are less precise. For example, the amygdala has strong and widely distributed connections with the TP, Thalamus,

Hippocampus, and PHG [13, 14, 17, 21, 22, 25, 26, 28-30]. However, connections with the MFG, PCC, and Precuneus are weaker and more restricted [15, 16, 18, 19, 29, 31]. Our data also showed that ipsilateral ROIs of the DMN modulated by neurofeedback are mainly connected with the central and basal nuclei. These nuclei are central for processing fear and anxiety [75-77], which are mediated by amygdala connections with regions processing context-specific aspects of the stress response [78, 79]. Modulation of fear and stress may play an essential role in worry and rumination, symptoms significantly correlated with amygdala rsFC with some DMN ROIs, including the MFG and precuneus [80].

Importantly, the ROIs listed in this study are specific to some but not all nodes of the SN and DMN. For example, regions like the ventral striatum (SN node) and vmPFC (DMN node) did not change rsFC with the amygdala after neurofeedback. These regions are known to be anatomically interconnected with the amygdala [15, 23, 24, 27, 29, 30, 32-34]. Although not identified in the rsFC studies, additional evidence suggests these regions are relevant during the neurofeedback task. The ventral striatum is highly active during neurofeedback reward processing [1]. Additionally, amygdala connectivity with the vmPFC changes during neurofeedback training [11, 81]. Thus, amygdala neurofeedback is associated with a modulation of the SN and DMN through anatomical connections.

Our data showed no monosynaptic connections from the amygdala to the contralateral ROIs, consistent with previous studies in the literature [82]. However, the amygdala is tightly linked with the ipsilateral hippocampus and PHG [14, 26, 28], which are connected to the contralateral structures [83-85]. Importantly, all studies included in our analysis [5, 12, 35] used a protocol based on positive autobiographical memory recall to up-regulate the BOLD signal of the left amygdala [11]. Neurofeedback studies using this protocol reported the hippocampus and PHG coactivation during the neurofeedback training task [11, 36, 37], increased functional connectivity between the left amygdala and left hippocampal/PHG structures [11, 12], and increased gray matter volume of hippocampal subfields [55]. Complementarily, neurofeedback targeting the up-regulation of the left hippocampus during autobiographical memory recall also leads to co-activation of the amygdala and increased amygdala-hippocampus functional connectivity [86]. Together with our anatomical delineation, these results suggest that rsFC changes with the contralateral DMN ROIs could be explained via amygdala-hippocampal projections.

Neuroanatomical basis of clinical effects

The studies providing the ROI coordinates [5, 12, 35] are follow-up investigations from original trials with patients with depression [36, 87] or PTSD [88]. These patients showed significant clinical improvement and reduced symptoms after neurofeedback training [36, 87, 88]. Notably, around 30% of patients with depression reached

remission levels at the primary endpoint [87]. These clinical effects correlated with the normalization of rsFC over the days following the neurofeedback training [5], similar to the effect observed in other protocols [6]. Thus, these clinical effects of fMRI neurofeedback training are likely to be associated with the rebalance of abnormal functional connections.

Monosynaptic connections allow the amygdala to modulate the ROIs of the SN and DMN quickly during neurofeedback sessions. A similar process to what is observed during focal stimulation of the amygdala [69, 89]: after systematic reinforcement, changes in these connections are sustained beyond the task and observed at rest [5, 12, 35]. These long-lasting connectivity changes may lead to synaptic rebalance and consequent clinical improvement, as observed in common pharmacological interventions [90].

Technical considerations

Anatomical tract-tracing is the gold standard method for delineating connections in the primate brain [91]. However, our tracer data showed inconsistent labeling between the amygdala and lateral precuneus. In both cases, only retrograde labeling was identified. Proper tracer labeling in long-distance pathways may require up to 5 weeks of transport time [92, 93], while our cases were perfused after two weeks. Thus, a possible explanation is that the anterograde transport may need longer transport time to show labeling in long-distance connections. These transport characteristics should be considered in future studies.

For both species, we used submillimeter dMRI datasets (500 μm in NHPs and 760 μm in humans) to delineate bundles that would be inaccessible at lower-resolution [94]. However, even at the submillimeter scale, the reconstruction of some anatomical connections identified in the tracer data was challenging in the dMRI data. For example, very few streamlines were identified linking the amygdala and the LPFC in both species. However, NHP tracer data show amygdala projections traveling through the uncinate fasciculus to reach their targets in the ventrolateral prefrontal cortex [95, 96], with similar fiber organization in the human brain [97]. In both species, dMRI data also showed false positive connections with the contralateral hemisphere. Some of these contralateral connections identified using dMRI are likely caused by the proximity of the fornix to actual amygdala pathways, such as the stria terminalis (<700 μm). In fact, studies trying to separate these bundles also reported the partial volume effects in their tract reconstructions [98, 99]. Therefore, the combined analysis of NHP tract tracing and NHP and human dMRI data is essential for delineating circuits relevant to neuroimaging studies [91] and identifying challenging fiber configurations for tractography algorithms [100-102].

Conclusion and Future Perspectives

We described the neuroanatomical circuits involved in rsFC changes following amygdala neurofeedback training. We showed that neurofeedback modulates the SN and DMN through monosynaptic connections from the targeted region providing real-time feedback (amygdala) and disynaptic connections with areas involved in the targeted cognitive process (hippocampus and PHG during autobiographical memory recall). Such circuitry allows for rapid modulation and reinforcement of amygdala connections with large-scale networks, leading to clinical improvements observed in the literature. This new mechanistic hypothesis should be probed in future human and animal studies. Moreover, our approach (combining NHP tract-tracing and dMRI *ex vivo* and human dMRI *in vivo*) can also guide future clinical neurofeedback experiments. For instance, it allows the identification of amygdala nuclei for targeting with neurofeedback at high field (e.g., as those achievable at 7T). It can also select alternative targets within the anatomical circuit to optimize neurofeedback for non-responders to the amygdala modulation.

Acknowledgments

LT was supported by the Jonathan Edward Brooking Mental Health Research Fellowship and NIH grant K99-MH130648. LT, JL, and SH were partially supported by NIH grants P50-MH106435 and R01-MH045573. CM, ED, and AY were partially supported by NIH grants R01-NS119911 and R01-EB021265.

Financial Disclosures

The authors have no biomedical financial interests or potential conflicts of interest to report.

References

[1] R. Sitaram *et al.*, "Closed-loop brain training: the science of neurofeedback," *Nat Rev Neurosci,* vol. 18, no. 2, pp. 86-100, Feb 2017, doi: 10.1038/nrn.2016.164.

[2] R. T. Thibault, A. MacPherson, M. Lifshitz, R. R. Roth, and A. Raz, "Neurofeedback with fMRI: A critical systematic review," *Neuroimage,* vol. 172, pp. 786-807, May 15 2018, doi: 10.1016/j.neuroimage.2017.12.071.

[3] E. Dudek and D. Dodell-Feder, "The efficacy of real-time functional magnetic resonance imaging neurofeedback for psychiatric illness: A meta-analysis of brain and behavioral outcomes," *Neurosci Biobehav Rev,* vol. 121, pp. 291-306, Feb 2021, doi: 10.1016/j.neubiorev.2020.12.020.

[4] A. Tursic, J. Eck, M. Luhrs, D. E. J. Linden, and R. Goebel, "A systematic review of fMRI neurofeedback reporting and effects in clinical populations," *Neuroimage Clin,* vol. 28, p. 102496, 2020, doi: 10.1016/j.nicl.2020.102496.

[5] H. Yuan, K. D. Young, R. Phillips, V. Zotev, M. Misaki, and J. Bodurka, "Resting-state functional connectivity modulation and sustained changes after real-time functional magnetic resonance imaging neurofeedback training in depression," *Brain Connect,* vol. 4, no. 9, pp. 690-701, Nov 2014, doi: 10.1089/brain.2014.0262.

[6] M. Rance *et al.*, "Time course of clinical change following neurofeedback," *Neuroimage,* vol. 181, pp. 807-813, Nov 1 2018, doi: 10.1016/j.neuroimage.2018.05.001.

[7] P. Linhartova, A. Latalova, B. Kosa, T. Kasparek, C. Schmahl, and C. Paret, "fMRI neurofeedback in emotion regulation: A literature review," *Neuroimage,* vol. 193, pp. 75-92, Jun 2019, doi: 10.1016/j.neuroimage.2019.03.011.

[8] N. Goldway *et al.*, "Feasibility and utility of amygdala neurofeedback," *Neurosci Biobehav Rev,* vol. 138, p. 104694, Jul 2022, doi: 10.1016/j.neubiorev.2022.104694.

[9] V. Zotev, R. Phillips, K. D. Young, W. C. Drevets, and J. Bodurka, "Prefrontal control of the amygdala during real-time fMRI neurofeedback training of emotion regulation," *PLoS One,* vol. 8, no. 11, p. e79184, 2013, doi: 10.1371/journal.pone.0079184.

[10] A. A. Nicholson *et al.*, "The neurobiology of emotion regulation in posttraumatic stress disorder: Amygdala downregulation via real-time fMRI neurofeedback," *Hum Brain Mapp,* vol. 38, no. 1, pp. 541-560, Jan 2017, doi: 10.1002/hbm.23402.

[11] V. Zotev *et al.*, "Self-regulation of amygdala activation using real-time FMRI neurofeedback," *PLoS One,* vol. 6, no. 9, p. e24522, 2011, doi: 10.1371/journal.pone.0024522.

[12] K. D. Young *et al.*, "Altered task-based and resting-state amygdala functional connectivity following real-time fMRI amygdala neurofeedback training in major depressive disorder," *Neuroimage Clin,* vol. 17, pp. 691-703, 2018, doi: 10.1016/j.nicl.2017.12.004.

[13] J. P. Aggleton and M. Mishkin, "Projections of the amygdala to the thalamus in the cynomolgus monkey," *J. Comp. Neurol.,* vol. 222, no. 1, pp. 56-68, Jan 1 1984, doi: 10.1002/cne.902220106.

[14] J. P. Aggleton, "A description of the amygdalo-hippocampal interconnections in the macaque monkey," *Experimental Brain Research,* vol. 64, no. 3, pp. 515-26, 1986. [Online]. Available: http://www.ncbi.nlm.nih.gov/pubmed/3803489.

[15] J. P. Aggleton, N. F. Wright, D. L. Rosene, and R. C. Saunders, "Complementary Patterns of Direct Amygdala and Hippocampal Projections to the Macaque Prefrontal Cortex," *Cereb Cortex,* vol. 25, no. 11, pp. 4351-73, Nov 2015, doi: 10.1093/cercor/bhv019.

[16] D. G. Amaral and J. L. Price, "Amygdalo-cortical projections in the monkey *(Macaca fascicularis)*," *J. Comp. Neurol.,* vol. 230, pp. 465-496, 1984, doi: 10.1002/cne.902300402.

[17] D. G. Amaral and R. Insausti, "Retrograde transport of D-[3H]-aspartate injected into the monkey amygdaloid complex," *Experimental Brain Research,* vol. 88, no. 2, pp. 375-388, 1992/02/01 1992, doi: 10.1007/BF02259113.

[18] J. S. Baizer, R. Desimone, and L. G. Ungerleider, "Comparison of subcortical connections of inferior temporal and posterior parietal cortex in monkeys," *Visual neuroscience,* vol. 10, no. 1, pp. 59-72, 1993.

[19] H. Barbas and J. de Olmos, "Projections from the amygdala to basoventral and mediodorsal prefrontal regions in the Rhesus monkey," *J. Comp. Neurol.,* vol. 300, pp. 549-571, 1990.

[20] S. T. Carmichael and J. L. Price, "Limbic connections of the orbital and medial prefrontal cortex in macaque monkeys," *Journal of Comparative Neurology,* vol. 363, no. 4, pp. 615-641, Dec 25 1995, doi: 10.1002/cne.903630408.

[21] C. Elorette, P. A. Forcelli, R. C. Saunders, and L. Malkova, "Colocalization of tectal inputs with amygdala-projecting neurons in the macaque pulvinar," *Frontiers in neural circuits,* vol. 12, p. 91, 2018.

[22] H. T. Ghashghaei and H. Barbas, "Pathways for emotion: interactions of prefrontal and anterior temporal pathways in the amygdala of the rhesus monkey," *Neuroscience,* vol. 115, no. 4, pp. 1261-79, 2002. [Online]. Available: http://www.ncbi.nlm.nih.gov/entrez/query.fcgi?cmd=Retrieve&db=PubMed&dopt=Citation&list_uids=12453496.

[23] E. A. Kelly, V. K. Thomas, A. Indraghanty, and J. L. Fudge, "Perigenual and Subgenual Anterior Cingulate Afferents Converge on Common Pyramidal Cells in Amygdala Subregions of the Macaque," *J Neurosci,* Oct 14 2021, doi: 10.1523/JNEUROSCI.1056-21.2021.

[24] Y. Kim, H. Sakata, M. Nejime, N. Konoike, S. Miyachi, and K. Nakamura, "Afferent connections of the dorsal, perigenual, and subgenual anterior cingulate cortices of the monkey: amygdalar inputs and intrinsic connections," *Neuroscience Letters,* vol. 681, pp. 93-99, 2018.

[25] L. M. Romanski, M. Giguere, J. F. Bates, and P. S. Goldman-Rakic, "Topographic organization of medial pulvinar connections with the prefrontal cortex in the rhesus monkey," *Journal of Comparative Neurology,* vol. 379, no. 3, pp. 313-32, 1997.

[26] R. C. Saunders, D. L. Rosene, and G. W. Van Hoesen, "Comparison of the efferents of the amygdala and the hippocampal formation in the rhesus monkey: II. Reciprocal and non-reciprocal connections," *J. Comp. Neurol.,* vol. 271, pp. 185-207, 1988.

[27] K. K. Sharma, E. A. Kelly, C. W. Pfeifer, and J. L. Fudge, "Translating Fear Circuitry: Amygdala Projections to Subgenual and Perigenual Anterior Cingulate in the Macaque," *Cereb Cortex,* vol. 30, no. 2, pp. 550-562, Mar 21 2020, doi: 10.1093/cercor/bhz106.

[28] L. Stefanacci, W. A. Suzuki, and D. G. Amaral, "Organization of connections between the amygdaloid complex and the perirhinal and parahippocampal cortices in macaque monkeys," *Journal of Comparative Neurology,* vol. 375, no. 4, pp. 552-82, 1996.

[29] L. Stefanacci and D. G. Amaral, "Topographic organization of cortical inputs to the lateral nucleus of the macaque monkey amygdala: a retrograde tracing study," *Journal of Comparative Neurology,* vol. 421, no. 1, pp. 52-79, 2000.

[30] L. Stefanacci and D. G. Amaral, "Some observations on cortical inputs to the macaque monkey amygdala: an anterograde tracing study," *J Comp Neurol,* vol. 451, no. 4, pp. 301-23, Sep 30 2002. [Online]. Available: http://www.ncbi.nlm.nih.gov/entrez/query.fcgi?cmd=Retrieve&db=PubMed&dopt=Citation&list_uids=12210126.

[31] J. Buckwalter, C. Schumann, and G. Van Hoesen, "Evidence for direct projections from the basal nucleus of the amygdala to retrosplenial cortex in the Macaque monkey," *Experimental brain research,* vol. 186, pp. 47-57, 2008.

[32] S. N. Haber, D. P. Wolfe, and H. J. Groenewegen, "The relationship between ventral striatal efferent fibers and the distribution of peptide-positive woolly fibers in the forebrain of the rhesus monkey," (in English), *Neuroscience,* vol. 39, no. 2, pp. 323-38, 1990, doi: 10.1016/0306-4522(90)90271-5.

[33] J. L. Fudge, K. Kunishio, P. Walsh, C. Richard, and S. N. Haber, "Amygdaloid projections to ventromedial striatal subterritories in the primate," *Neuroscience,* vol. 110, no. 2, pp. 257-75, 2002, doi: 10.1016/s0306-4522(01)00546-2.

[34] J. L. Fudge, M. A. Breitbart, and C. McClain, "Amygdaloid inputs define a caudal component of the ventral striatum in primates," (in eng), *J Comp Neurol,* vol. 476, no. 4, pp. 330-47, Aug 30 2004, doi: 10.1002/cne.20228.

[35] M. Misaki *et al.*, "Real-time fMRI amygdala neurofeedback positive emotional training normalized resting-state functional connectivity in combat veterans with and without

PTSD: a connectome-wide investigation," (in English), *Neuroimage-Clinical,* vol. 20, pp. 543-555, 2018, doi: 10.1016/j.nicl.2018.08.025.

[36] K. D. Young *et al.*, "Real-time FMRI neurofeedback training of amygdala activity in patients with major depressive disorder," *PLoS One,* vol. 9, no. 2, p. e88785, 2014, doi: 10.1371/journal.pone.0088785.

[37] N. Liu, L. Yao, and X. Zhao, "Evaluating the amygdala network induced by neurofeedback training for emotion regulation using hierarchical clustering," *Brain Research,* vol. 1740, p. 146853, 2020.

[38] J. L. Lancaster *et al.*, "Bias between MNI and Talairach coordinates analyzed using the ICBM-152 brain template," *Human brain mapping,* vol. 28, no. 11, pp. 1194-1205, 2007.

[39] R. Kotter and E. Wanke, "Mapping brains without coordinates," *Philos Trans R Soc Lond B Biol Sci,* vol. 360, no. 1456, pp. 751-66, Apr 29 2005, doi: 10.1098/rstb.2005.1625.

[40] E. Y. Choi, Y. Tanimura, P. R. Vage, E. H. Yates, and S. N. Haber, "Convergence of prefrontal and parietal anatomical projections in a connectional hub in the striatum," *Neuroimage,* vol. 146, pp. 821-832, Feb 1 2017, doi: 10.1016/j.neuroimage.2016.09.037.

[41] W. Tang *et al.*, "A connectional hub in the rostral anterior cingulate cortex links areas of emotion and cognitive control," *Elife,* vol. 8, Jun 19 2019, doi: 10.7554/eLife.43761.

[42] L. R. Trambaiolli *et al.*, "Anatomical and functional connectivity support the existence of a salience network node within the caudal ventrolateral prefrontal cortex," *Elife,* vol. 11, p. e736344, May 5 2022, doi: 10.7554/eLife.76334.

[43] J. Veraart, D. S. Novikov, D. Christiaens, B. Ades-Aron, J. Sijbers, and E. Fieremans, "Denoising of diffusion MRI using random matrix theory," *Neuroimage,* vol. 142, pp. 394-406, 2016.

[44] E. Kellner, B. Dhital, V. G. Kiselev, and M. Reisert, "Gibbs-ringing artifact removal based on local subvoxel-shifts," *Magnetic resonance in medicine,* vol. 76, no. 5, pp. 1574-1581, 2016.

[45] S. B. Vos, C. M. Tax, P. R. Luijten, S. Ourselin, A. Leemans, and M. Froeling, "The importance of correcting for signal drift in diffusion MRI," *Magnetic resonance in medicine,* vol. 77, no. 1, pp. 285-299, 2017.

[46] J. L. Andersson, M. S. Graham, E. Zsoldos, and S. N. Sotiropoulos, "Incorporating outlier detection and replacement into a non-parametric framework for movement and distortion correction of diffusion MR images," *Neuroimage,* vol. 141, pp. 556-572, 2016.

[47] J. D. Tournier *et al.*, "MRtrix3: A fast, flexible and open software framework for medical image processing and visualisation," *Neuroimage,* vol. 202, p. 116137, Nov 15 2019, doi: 10.1016/j.neuroimage.2019.116137.

[48] T. Dhollander, R. Mito, D. Raffelt, and A. Connelly, "Improved white matter response function estimation for 3-tissue constrained spherical deconvolution," in *Proc. Intl. Soc. Mag. Reson. Med*, 2019, vol. 555, no. 10.

[49] K. S. Saleem *et al.*, "High-resolution mapping and digital atlas of subcortical regions in the macaque monkey based on matched MAP-MRI and histology," *Neuroimage,* vol. 245, p. 118759, 2021.

[50] M. Reuter, H. D. Rosas, and B. Fischl, "Highly accurate inverse consistent registration: a robust approach," *Neuroimage,* vol. 53, no. 4, pp. 1181-96, Dec 2010, doi: 10.1016/j.neuroimage.2010.07.020.

[51] F. Wang *et al.*, "In vivo human whole-brain Connectom diffusion MRI dataset at 760 µm isotropic resolution," *Scientific data,* vol. 8, no. 1, pp. 1-12, 2021.

[52] A. M. Dale, B. Fischl, and M. I. Sereno, "Cortical surface-based analysis. I. Segmentation and surface reconstruction," (in eng), *Neuroimage,* vol. 9, no. 2, pp. 179-94, Feb 1999, doi: 10.1006/nimg.1998.0395.

[53] B. Fischl, M. I. Sereno, and A. M. Dale, "Cortical surface-based analysis. II: Inflation, flattening, and a surface-based coordinate system," (in eng), *Neuroimage,* vol. 9, no. 2, pp. 195-207, Feb 1999, doi: 10.1006/nimg.1998.0396.

[54] B. Fischl *et al.*, "Automatically parcellating the human cerebral cortex," (in eng), *Cereb Cortex,* Research Support, Non-U.S. Gov't
Research Support, U.S. Gov't, P.H.S. vol. 14, no. 1, pp. 11-22, Jan 2004. [Online]. Available: http://www.ncbi.nlm.nih.gov/pubmed/14654453.

[55] M. Misaki *et al.*, "Hippocampal volume recovery with real-time functional MRI amygdala neurofeedback emotional training for posttraumatic stress disorder," *Journal of Affective Disorders,* vol. 283, pp. 229-235, 2021.

[56] K. D. Young, V. Zotev, R. Phillips, M. Misaki, W. C. Drevets, and J. Bodurka, "Amygdala real-time functional magnetic resonance imaging neurofeedback for major depressive disorder: A review," *Psychiatry and clinical neurosciences,* vol. 72, no. 7, pp. 466-481, 2018.

[57] N. Goldway *et al.*, "Feasibility and Utility of Amygdala NeuroFeedback," *Neuroscience & Biobehavioral Reviews,* p. 104694, 2022.

[58] A. A. Nicholson *et al.*, "The neurobiology of emotion regulation in posttraumatic stress disorder: Amygdala downregulation via real-time fMRI neurofeedback," *Human Brain Mapping,* vol. 38, no. 1, pp. 541-560, 2017.

[59] M. Petrides, F. Tomaiuolo, E. H. Yeterian, and D. N. Pandya, "The prefrontal cortex: comparative architectonic organization in the human and the macaque monkey brains," (in eng), *Cortex,* Comparative Study
Research Support, Non-U.S. Gov't
Review vol. 48, no. 1, pp. 46-57, Jan 2012, doi: 10.1016/j.cortex.2011.07.002.

[60] A. Goulas, M. Bastiani, G. Bezgin, H. B. Uylings, A. Roebroeck, and P. Stiers, "Comparative analysis of the macroscale structural connectivity in the macaque and human brain," *PLoS Comput Biol,* vol. 10, no. 3, p. e1003529, Mar 2014, doi: 10.1371/journal.pcbi.1003529.

[61] A. Touroutoglou *et al.*, "A ventral salience network in the macaque brain," *Neuroimage,* vol. 132, pp. 190-197, May 15 2016, doi: 10.1016/j.neuroimage.2016.02.029.

[62] D. Mantini *et al.*, "Default mode of brain function in monkeys," (in eng), *J Neurosci,* Meta-Analysis
Research Support, N.I.H., Extramural
Research Support, Non-U.S. Gov't
Research Support, U.S. Gov't, Non-P.H.S.
Review vol. 31, no. 36, pp. 12954-62, Sep 7 2011, doi: 10.1523/JNEUROSCI.2318-11.2011.

[63] J. L. Vincent *et al.*, "Intrinsic functional architecture in the anaesthetized monkey brain," (in eng), *Nature,* Research Support, N.I.H., Extramural
Research Support, Non-U.S. Gov't
Research Support, U.S. Gov't, Non-P.H.S. vol. 447, no. 7140, pp. 83-6, May 3 2007, doi: 10.1038/nature05758.

[64] L. J. Porrino, A. M. Crane, and P. S. Goldman-Rakic, "Direct and indirect pathways from the amygdala to the frontal lobe in rhesus monkeys," *J. Comp. Neurol.,* vol. 198, pp. 121-136, 1981.

[65] K. D. Young, V. Zotev, R. Phillips, M. Misaki, W. C. Drevets, and J. Bodurka, "Amygdala real-time functional magnetic resonance imaging neurofeedback for major depressive disorder: A review," *Psychiatry Clin Neurosci,* vol. 72, no. 7, pp. 466-481, Jul 2018, doi: 10.1111/pcn.12665.

[66] K. L. Hoffman, K. M. Gothard, M. C. Schmid, and N. K. Logothetis, "Facial-expression and gaze-selective responses in the monkey amygdala," *Curr Biol,* vol. 17, no. 9, pp. 766-72, May 1 2007, doi: 10.1016/j.cub.2007.03.040.

[67] K. M. Gothard, F. P. Battaglia, C. A. Erickson, K. M. Spitler, and D. G. Amaral, "Neural responses to facial expression and face identity in the monkey amygdala," *J Neurophysiol,* vol. 97, no. 2, pp. 1671-83, Feb 2007, doi: 10.1152/jn.00714.2006.

[68] O. Dal Monte, V. D. Costa, P. L. Noble, E. A. Murray, and B. B. Averbeck, "Amygdala lesions in rhesus macaques decrease attention to threat," *Nat Commun,* vol. 6, no. 1, p. 10161, Dec 14 2015, doi: 10.1038/ncomms10161.

[69] S. Shi *et al.*, "Infrared neural stimulation with 7T fMRI: A rapid in vivo method for mapping cortical connections of primate amygdala," *Neuroimage,* vol. 231, p. 117818, May 1 2021, doi: 10.1016/j.neuroimage.2021.117818.

[70] J. P. Royet *et al.*, "Emotional responses to pleasant and unpleasant olfactory, visual, and auditory stimuli: a positron emission tomography study," *J Neurosci,* vol. 20, no. 20, pp. 7752-9, Oct 15 2000, doi: 10.1523/JNEUROSCI.20-20-07752.2000.

[71] K. Sergerie, C. Chochol, and J. L. Armony, "The role of the amygdala in emotional processing: a quantitative meta-analysis of functional neuroimaging studies," *Neurosci Biobehav Rev,* vol. 32, no. 4, pp. 811-30, 2008, doi: 10.1016/j.neubiorev.2007.12.002.

[72] A. K. Anderson and E. A. Phelps, "Lesions of the human amygdala impair enhanced perception of emotionally salient events," *Nature,* vol. 411, no. 6835, pp. 305-9, May 17 2001, doi: 10.1038/35077083.

[73] R. Adolphs, D. Tranel, H. Damasio, and A. R. Damasio, "Fear and the human amygdala," *J. Neurosci.,* vol. 15(9), no. 9, pp. 5879-5891, Sep 1995. [Online]. Available: http://www.ncbi.nlm.nih.gov/pubmed/7666173.

[74] R. Graham, O. Devinsky, and K. S. Labar, "Quantifying deficits in the perception of fear and anger in morphed facial expressions after bilateral amygdala damage," *Neuropsychologia,* vol. 45, no. 1, pp. 42-54, Jan 7 2007, doi: 10.1016/j.neuropsychologia.2006.04.021.

[75] A. S. Fox *et al.*, "Central amygdala nucleus (Ce) gene expression linked to increased trait-like Ce metabolism and anxious temperament in young primates," *Proc Natl Acad Sci U S A,* vol. 109, no. 44, pp. 18108-13, Oct 30 2012, doi: 10.1073/pnas.1206723109.

[76] P. H. Roseboom *et al.*, "Neuropeptide Y receptor gene expression in the primate amygdala predicts anxious temperament and brain metabolism," *Biol Psychiatry,* vol. 76, no. 11, pp. 850-7, Dec 1 2014, doi: 10.1016/j.biopsych.2013.11.012.

[77] N. H. Kalin, S. E. Shelton, and R. J. Davidson, "The role of the central nucleus of the amygdala in mediating fear and anxiety in the primate," *J Neurosci,* vol. 24, no. 24, pp. 5506-15, Jun 16 2004, doi: 10.1523/JNEUROSCI.0292-04.2004.

[78] D. G. Amaral, J. L. Price, A. Pitkanen, and S. T. Carmichael, "Anatomical organization of the primate amygdaloid complex," in *The Amygdala: Neurobiological Aspects of Emotion, Memory, and Mental Dysfunction*: Wiley-Liss, Inc., 1992, pp. 1-66.

[79] M. Davis, "The role of the amygdala in fear and anxiety," *Annual review of neuroscience,* vol. 15, no. 1, pp. 353-375, 1992.

[80] C. Feurer *et al.*, "Resting state functional connectivity correlates of rumination and worry in internalizing psychopathologies," *Depress Anxiety,* vol. 38, no. 5, pp. 488-497, May 2021, doi: 10.1002/da.23142.

[81] C. Paret *et al.*, "Alterations of amygdala-prefrontal connectivity with real-time fMRI neurofeedback in BPD patients," *Soc Cogn Affect Neurosci,* vol. 11, no. 6, pp. 952-60, Jun 2016, doi: 10.1093/scan/nsw016.

[82] S. Demeter, D. L. Rosene, and G. W. Van Hoesen, "Fields of origin and pathways of the interhemispheric commissures in the temporal lobe of macaques," *J Comp Neurol,* vol. 302, no. 1, pp. 29-53, Dec 1 1990, doi: 10.1002/cne.903020104.

[83] S. Demeter, D. L. Rosene, and G. W. Van Hoesen, "Interhemispheric pathways of the hippocampal formation, presubiculum, and entorhinal and posterior parahippocampal

cortices in the rhesus monkey: The structure and organization of the hippocampal commissures," *J. Comp. Neurol.,* vol. 233, pp. 30-47, 1985.

[84] J. P. Aggleton, R. Desimone, and M. Mishkin, "The origin, course, and termination of the hippocampothalamic projections in the macaque," *Journal of Comparative Neurology,* vol. 243, no. 3, pp. 409-21, Jan 15 1986, doi: 10.1002/cne.902430310.

[85] M. L. Mathiasen, R. C. Louch, A. D. Nelson, C. M. Dillingham, and J. P. Aggleton, "Trajectory of hippocampal fibres to the contralateral anterior thalamus and mammillary bodies in rats, mice, and macaque monkeys," *Brain Neurosci Adv,* vol. 3, p. 2398212819871205, 2019, doi: 10.1177/2398212819871205.

[86] Y. Zhu *et al.*, "Emotion Regulation of Hippocampus Using Real-Time fMRI Neurofeedback in Healthy Human," *Front Hum Neurosci,* vol. 13, p. 242, 2019, doi: 10.3389/fnhum.2019.00242.

[87] K. D. Young *et al.*, "Randomized Clinical Trial of Real-Time fMRI Amygdala Neurofeedback for Major Depressive Disorder: Effects on Symptoms and Autobiographical Memory Recall," *Am J Psychiatry,* vol. 174, no. 8, pp. 748-755, Aug 1 2017, doi: 10.1176/appi.ajp.2017.16060637.

[88] V. Zotev *et al.*, "Real-time fMRI neurofeedback training of the amygdala activity with simultaneous EEG in veterans with combat-related PTSD," *Neuroimage Clin,* vol. 19, pp. 106-121, 2018, doi: 10.1016/j.nicl.2018.04.010.

[89] D. Folloni *et al.*, "Manipulation of Subcortical and Deep Cortical Activity in the Primate Brain Using Transcranial Focused Ultrasound Stimulation," *Neuron,* vol. 101, no. 6, pp. 1109-1116 e5, Mar 20 2019, doi: 10.1016/j.neuron.2019.01.019.

[90] C. J. Harmer, R. S. Duman, and P. J. Cowen, "How do antidepressants work? New perspectives for refining future treatment approaches," *The Lancet Psychiatry,* vol. 4, no. 5, pp. 409-418, 2017.

[91] S. N. Haber *et al.*, "Circuits, Networks, and Neuropsychiatric Disease: Transitioning From Anatomy to Imaging," *Biol Psychiatry,* vol. 87, no. 4, pp. 318-327, Feb 15 2020, doi: 10.1016/j.biopsych.2019.10.024.

[92] K. Keizer and H. G. Kuypers, "Distribution of corticospinal neurons with collaterals to the lower brain stem reticular formation in monkey (Macaca fascicularis)," *Exp Brain Res,* vol. 74, no. 2, pp. 311-8, 1989. [Online]. Available: http://www.ncbi.nlm.nih.gov/entrez/query.fcgi?cmd=Retrieve&db=PubMed&dopt=Citation&list_uids=2924851

[93] J. L. Lanciego and F. G. Wouterlood, "Neuroanatomical tract-tracing techniques that did go viral," (in English), *Brain Structure & Function,* vol. 225, no. 4, pp. 1193-1224, May 2020, doi: 10.1007/s00429-020-02041-6.

[94] C. Maffei, S. Wang, S. Haber, and A. Yendiki, "Submillimeter dMRI protocol optimization for accurate in-vivo reconstruction of deep-brain circuitry," *Proc. Intl. Soc. Mag. Res. Med.,* 2022.

[95] J. F. Lehman, B. D. Greenberg, C. C. McIntyre, S. A. Rasmussen, and S. N. Haber, "Rules ventral prefrontal cortical axons use to reach their targets: implications for diffusion tensor imaging tractography and deep brain stimulation for psychiatric illness," (in eng), *J Neurosci,* vol. 31, no. 28, pp. 10392-402, Jul 13 2011, doi: 10.1523/JNEUROSCI.0595-11.2011.

[96] W. J. H. Nauta, "Fibre degeneration following lesions of the amygdaloid complex in the monkey," *J. Anat.,* vol. 95, pp. 515-531, 1961. [Online]. Available: http://www.ncbi.nlm.nih.gov/pmc/articles/PMC1244065.

[97] S. Jbabdi, J. F. Lehman, S. N. Haber, and T. E. Behrens, "Human and monkey ventral prefrontal fibers use the same organizational principles to reach their targets: tracing versus tractography," *J Neurosci,* vol. 33, no. 7, pp. 3190-201, Feb 13 2013, doi: 10.1523/JNEUROSCI.2457-12.2013.

[98] H. G. Kwon, W. M. Byun, S. H. Ahn, S. M. Son, and S. H. Jang, "The anatomical characteristics of the stria terminalis in the human brain: a diffusion tensor tractography study," (in eng), *Neurosci Lett,* Research Support, Non-U.S. Gov't vol. 500, no. 2, pp. 99-102, Aug 15 2011, doi: 10.1016/j.neulet.2011.06.013.

[99] A. Kamali *et al.*, "Mapping the trajectory of the stria terminalis of the human limbic system using high spatial resolution diffusion tensor tractography," *Neuroscience Letters,* vol. 608, pp. 45-50, 2015.

[100] G. Grisot, S. N. Haber, and A. Yendiki, "Diffusion MRI and anatomic tracing in the same brain reveal common failure modes of tractography," *Neuroimage,* vol. 239, p. 118300, Oct 1 2021, doi: 10.1016/j.neuroimage.2021.118300.

[101] C. Maffei *et al.*, "Insights from the IronTract challenge: Optimal methods for mapping brain pathways from multi-shell diffusion MRI," *Neuroimage,* vol. 257, p. 119327, Aug 15 2022, doi: 10.1016/j.neuroimage.2022.119327.

[102] A. Yendiki, M. Aggarwal, M. Axer, A. F. D. Howard, A. V. C. van Walsum, and S. N. Haber, "Post mortem mapping of connectional anatomy for the validation of diffusion MRI," *Neuroimage,* vol. 256, p. 119146, Aug 1 2022, doi: 10.1016/j.neuroimage.2022.119146.